BIOCHEMISTRY
including biophysical chemistry & molecular biology
Article

Biochemistry **2009,** *48,* 5813–5821 5813
DOI: 10.1021/bi9004599

Solution Structure of the HsapBK K^+ Channel Voltage-Sensor Paddle Sequence[†,‡]

Sofia Unnerståle, Jesper Lind, Evangelos Papadopoulos, and Lena Mäler*

Department of Biochemistry and Biophysics, Center for Biomembrane Research, The Arrhenius Laboratories for Natural Sciences, Stockholm University, SE-106 91 Stockholm, Sweden

Received March 17, 2009; Revised Manuscript Received May 19, 2009

ABSTRACT: Voltage-gated potassium channels open and close in response to changes in the membrane potential. In this study, we have determined the NMR solution structure of the putative S3b−S4 voltage-sensor paddle fragment, the part that moves to mediate voltage gating, of the HsapBK potassium channel in dodecylphosphocholine (DPC) micelles. This paper presents the first structure of the S3b−S4 fragment from a BK channel. Diffusion coefficients as determined from PFG NMR experiments showed that a well-defined complex between the peptide and DPC molecules was formed. The structure reveals a helix−turn−helix motif, which is in agreement with crystal structures of other voltage-gated potassium channels, thus indicating that it is feasible to study the isolated fragment. The paddle motifs generally contain several basic residues, implicated in the gating. The critical Arg residues in this structure all reside on the surface, which is in agreement with crystal structures of K_v channels. Similarities in the structure of the S3b−S4 fragment in BK and K_v channels as well as important differences are seen, which may be important for explaining the details in paddle movement within a bilayer.

Potassium channels were originally described as the membrane proteins that, during an action potential, open their pore and allow a flow of K^+ ions out of the neuron, to further enhance the restoration of the resting potential, brought about by spontaneous inactivation of voltage-gated sodium channels (*1*). However, now it is known that potassium channels are involved in many physiological functions and can be found in all types of organisms and cells (*2*, *3*). Potassium channels are highly conserved: they are all tetrameric membrane proteins that specifically conduct K^+ through an aqueous pore. Structurally, potassium channels can be divided into two major classes: the six-transmembrane-helix voltage-gated (K_v) and the two-transmembrane-helix inward rectifiers (K_{ir}).

K_v channels are homotetramers (*4*) in which each subunit contains six transmembrane segments, S1−S6. Crystal structures of K_v and of a Shaker family K^+ channel have revealed that the K_v channels are composed of two structural units, the pore domain with the selectivity filter (segments S5 and S6) and the voltage-sensor domain (segments S1−S4) (*5*−*8*).

Calcium- and voltage-activated BK channels (known as MaxiK channels) also contain a S4 helix, but unlike K_v channels, they contain seven transmembrane helices (S0−S6) and a large cytosolic domain (S7−S10) (*9*). These channels are activated by both a voltage and cytoplasmic Ca^{2+}. They often colocalize with voltage-dependent calcium channels to dampen their excitatoric effect through negative feedback (*10*−*12*). The Ca^{2+} activation and the voltage activation act independently (*11*, *13*).

Within the voltage-sensor domain, the S4 segment is generally rich in Arg (or Lys) residues and forms a "paddle" motif with part of the S3 helix, S3b (*5*). This paddle motif provides a means for moving charges within the membrane and seems to be sensitive to the membrane potential (*5*, *14*). The gates of these proteins can thus be open or closed, depending on the voltage variations in the cell membrane. This voltage-sensor motif appears to be conserved within a wide range of channels (*15*−*19*). It has also been shown that the voltage-sensor motif can function as a voltage-activated proton channel without a separate pore domain (*17*−*19*). Crystal structures of several voltage-dependent potassium channels have been obtained, and the results have shown that the voltage-sensor paddle fragment, S3b−S4, moves within the membrane to open the pore (*5*−*8*, *20*−*22*). The crystal structures have further revealed that the paddle is composed of a helix−turn−helix motif. The paddle motif is rich in Arg residues, and the movement of these charges across the membrane is linked with pore gating (*23*, *24*). Many questions about the extent of the paddle motion within the membrane still remain, and different biophysical and biochemical techniques have been shown to give different results concerning the actual distance that the domain moves (*8*, *24*, *25*).

In this paper, we describe the high-resolution NMR solution structure of the voltage-sensor motif from the *Homo sapiens*

[†]This work was supported by The Swedish Research Council, The Carl Trygger Foundation, and the Magnus Bergvall Foundation.

[‡]The chemical shifts for HsapBK(233−260) in DPC micelles have been deposited in the BioMagResBank as entry 16112. The coordinates for the solution structure of HsapBK(233−260) in DPC micelles have been deposited in the Protein Data Bank as entry 2k44.

*To whom correspondence should be addressed. Phone: +46 8 162448. Fax: +46 8 155597. E-mail: lena.maler@dbb.su.se.

Published on Web 05/20/2009

BK K^+ channel, HsapBK(233−260).[1] It consists of 28 amino acid residues, with the sequence PVFVSVYLNRSWLGLRFLRALRLIQFSE. This sequence is totally conserved among BK channels of different types and from different species. On the other hand, the corresponding sequences in K_v channels appear not to be equally conserved, and hence, it is important to examine the structural differences and similarities between them. The membrane-bound structure of the fragment was obtained by reconstituting the peptide in dodecylphosphocholine (DPC) micelles. We demonstrate that the structure of the isolated motif does indeed fold into a helix−turn−helix motif. The structure will be helpful in future studies of the membrane interactions of the voltage-sensor motifs.

EXPERIMENTAL PROCEDURES

Sample Preparation. The voltage-sensor motif, HsapBK(233−260), was obtained as a custom synthesis from NeoMPS (Strasbourg, France) and used without further purification. Deuterated dodecylphosphocholine-d_{38} (DPC) was purchased from Cambridge Isotope Laboratories, Inc., while 1,2-dimyristoyl-*sn*-glycero-3-phosphocholine (DMPC-d_{54}) and 1,2-dihexanoyl-*sn*-glycero-3-phosphocholine (DHPC-d_{22}) were purchased from Avanti Polar Lipids, Inc. (Alabaster, AL).

For the ^{1}H NMR experiments and CD measurements, a sample containing 1 mM peptide was dissolved in 100 mM DPC-d_{38} (98%) and 50 mM potassium phosphate buffer (pH 5.5); 10% ^2H_2O was added for field/frequency lock stabilization in NMR experiments. A sample of 1 mM peptide in 300 mM, q = 0.25 (q is the concentration ratio of DMPC to DHPC) DMPC/DHPC bicelles was also prepared for CD measurements and initial NMR experiments. Bicelles were prepared by mixing lyophilized DMPC with a stock solution of DHPC (1 M) and phosphate buffer (final concentration of 50 mM, pH 5.8) to yield a total lipid concentration of 300 mM. Peptide dissolved in CH_3OH and $CHCl_3$ (1:3) was added to a freeze-dried bicelle solution; the mixture was freeze-dried yet again and subsequently dissolved in water.

CD Spectroscopy. CD spectra were recorded for HsapBK (233−260) in DPC and in a q = 0.25 DMPC/DHPC bicelle solution. CD measurements were acquired on a Chirascan CD spectrometer with a 0.1 mm quartz cell. The temperature was adjusted to 25 °C with a TC 125 temperature control. Wavelengths ranging from 190 to 250 nm were measured with a 1 nm step resolution. Spectra were collected and averaged over five measurements. Background spectra of the pure detergent solution and of the pure bicelle solution were subtracted from the peptide spectra.

Fluorescence Spectroscopy. Tryptophan fluorescence was measured on a Perkin-Elmer LS 50B luminescence spectrometer. All measurements where taken at room temperature in a quartz cuvette with a light path length of 2 mm. The excitation wavelength was 280 nm, and the emission was scanned from 300 to 500 nm. Ten scans were collected with a scan speed of 600 nm/min. The excitation bandwidth as well as the emission bandwidth was 10 nm.

NMR Spectroscopy. Two-dimensional ^{1}H NMR measurements were recorded on a Varian Inova spectrometer equipped with a triple-resonance probe head operating at a ^{1}H frequency of 800 MHz. Two-dimensional COSY (*26*, *27*), TOCSY (*28*), and NOESY (*29*) spectra were recorded for HsapBK(233−260) in 100 mM DPC. The TOCSY spectra were recorded with mixing times of 30, 55, and 80 ms, and the NOESY spectra were recorded with mixing times of 100, 150, and 300 ms. The 150 ms NOESY was used for assigning distance constraints, as described previously for structure determination of micelle-bound peptides (*30*). Spectra were typically collected as 2048−4096 × 320 data point matrices using 64−96 scans. Water suppression was achieved with the WATERGATE pulse sequence (*31*). The spectra were processed with NMRPipe version 2.3 (*32*), and spectral analysis was performed with Sparky 3 (*33*). All two-dimensional NMR experiments were performed at 37 °C.

Translational diffusion experiments were conducted on a Varian Inova spectrometer equipped with a triple-resonance probe head operating at a ^{1}H frequency of 600 MHz. Measurements were performed at 25 and 37 °C. Diffusion constants were determined for DPC in the monomer state using a 0.5 mM DPC sample, since the critical micelle concentration of DPC is 1 mM (*34*). Diffusion constants were measured using a modified Stejskal−Tanner spin−echo experiment (*35*−*37*) with a fixed diffusion time and a pulsed field gradient increasing linearly over 32 steps. To correct for field gradient inhomogeneity, the intensity decline for every experiment was fitted to a modified version of the Stejskal−Tanner equation (*38*). Viscosities of the samples were estimated by measuring the H_2O diffusion rates and comparing them to standard values in water (*39*), and the viscosity-corrected diffusion constants (*40*) could then be used to calculate hydrodynamic radii via the Stokes−Einstein relation using the assumption that the micelle is a hard sphere (*41*, *42*). A hydration layer with an estimated depth of 2.8 Å was assumed in the calculations.

Structure Calculation. Cross-peaks in the 150 ms mixing time NOESY spectrum were used for deriving distance constraints for calculating a solution structure for HsapBK(233−260) in DPC. In all, 327 distance constrains were assigned (160 intraresidue, 89 sequential, 72 medium-range, and 6 long-range constraints). The cross-peak intensities were initially converted to distances using routines in CYANA 2.0 (*43*). These distances were subsequently altered manually in several stages as described previously (*44*). Structures were generated using CYANA, applying standard annealing algorithms. Analyses of the structures, including analyses of secondary structure and backbone dihedral angles, were performed with PROCHECK NMR (*45*). A total of 100 structures were calculated, and a final ensemble of 25 structures was selected, on the basis of the CYANA target function, to represent the final solution structure. The coordinates of the final ensemble of structures have together with the distance constraints been deposited in the Protein Data Bank as entry 2k44. The chemical shift assignments have been deposited with the BMRB as entry 16112.

RESULTS

Interaction between HsapBK(233−260) and DPC. To determine the extent of structure in HsapBK(233−260) in various membrane mimetics, CD spectra were recorded between 190 and

[1]Abbreviations: HsapBK, *H. sapiens* BK K^+ channel; HsapBK(233−260), sequence P_{233}VFVSVYLNRSWLGLRFLRALRLIQFSE$_{260}$ derived from HsapBK; DPC, dodecylphosphocholine; CD, circular dichroism; NMR, nuclear magnetic resonance; NOESY, nuclear Overhauser effect spectroscopy; NOEs, proton−proton distances determined from NOESY cross-peaks; TOCSY, total correlation spectroscopy; rmsd, root-mean-square deviation; CMC, critical micelle concentration.

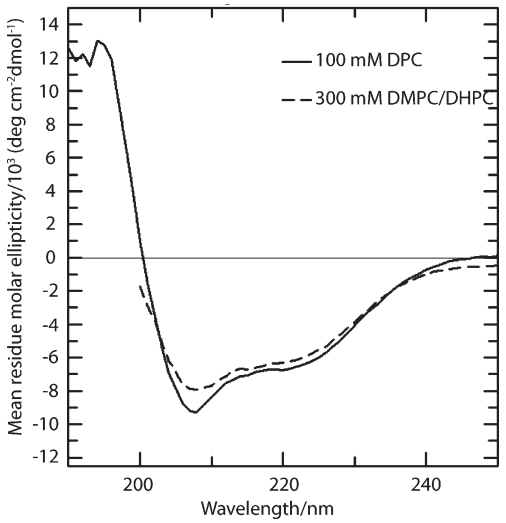

FIGURE 1: CD spectra recorded at 37 °C for 1 mM HsapBK(233−260) in 100 mM DPC (—) and in 300 mM, $q = 0.25$ DMPC/DHPC bicelles (– – –).

250 nm in 100 mM DPC and in a 300 mM DMPC/DHPC bicelle solution (Figure 1). Bicelles provide a bilayered environment, in which many proteins have been found to be active (*46*). It was difficult to measure the spectrum for the bicelle sample below 200 nm, and hence, only the spectrum between 200 and 250 nm is shown. This has previously been observed for peptides tightly bound to bicelles (*47*). It was also somewhat difficult to accurately measure the signal intensity for the peptide in the DPC sample below 195 nm.

Nevertheless, the spectra of the peptide in both $q = 0.25$ bicelle solution and DPC display the characteristic features of a helical structure, although the amplitude at 222 nm suggests that only ~30% of the sequence is structured. This may (in part) be due to difficulties in accurately estimating the peptide concentration. The similarity between the spectra indicates that the structure of the paddle motif is similar in the two membrane mimetic solvents, and that DPC provides an adequate membrane environment. Since the NMR spectra of the peptide in the bicelle solvent were hampered by large lipid signals and broad peptide resonances, DPC was subsequently chosen for performing the structural studies. The chemical shifts for the observable resonances in the peptide dissolved in the bicelle solution were, however, similar to those in DPC. Again, this indicates that the paddle fragment has a similar structure in DPC and in the bilayer bicelles.

The complex between DPC and the peptide was further analyzed by measuring translational diffusion coefficients for DPC as well as for the peptide at 25 and 37 °C (Table 1). The measurements at the lower temperature were made to ensure that the diffusion coefficients obtained at 37 °C were not influenced by a higher degree of convection currents in the sample. The calculated hydrodynamic radii did, however, not vary significantly within this temperature range.

The size of the peptide−DPC complex was examined from diffusion data. The peptide is only marginally soluble in aqueous solution and can thus be assumed to be fully bound to the DPC complex. Hence, on the basis of the diffusion rate of the peptide, a hydrodynamic radius of the DPC/peptide aggregates was calculated to 22.9 ± 0.3 Å at 37 °C.

To compare the size of the DPC/peptide aggregate to that of a DPC micelle, the size of the DPC micelle alone was estimated. A certain fraction of the DPC is dissolved as monomers in the solution, even above the CMC, and a weighted average between the monomer and the micelle diffusion is thus observed (*48*). Hence, we determined the diffusion rates for both monomeric DPC (below the CMC) and the DPC micelle sample. Using these values, we estimate that 3% of the total amount of DPC exists as free monomers and that the hydrodynamic radius for the DPC micelles without the peptide is 21.3 ± 0.3 Å, which corresponds well with previous results for DPC micelles (*49*, *50*).

Table 1: Diffusion Coefficients and Hydrodynamic Radii for DPC and HsapBK(233−260)

	D ($\times 10^{-11}$ m^2 s^{-1})[a]		
sample	DPC	HsapBK(233−260)	R_h (Å)[b]
	25 °C		
0.5 mM DPC	48.8 ± 0.3		1.9 ± 0.3
100 mM DPC	11.3 ± 0.2		20.6 ± 0.3
100 mM DPC and 1 mM HsapBK(233−260)	10.6 ± 0.1	9.3 ± 0.2	22.1 ± 0.4
	37 °C		
0.5 mM DPC	63.6 ± 0.4		2.4 ± 0.4
100 mM DPC	14.9 ± 0.2		21.3 ± 0.2
100 mM DPC and 1 mM HsapBK(233−260)	14.1 ± 0.4	12.8 ± 0.4	22.9 ± 0.4

[a] Normalized according to the diffusion of HDO to account for viscosity differences. [b] Hydrodynamic radius. For the DPC micelle sample, the fraction of free monomer in solution was taken into account. For the DPC−peptide complex, the radius was calculated from the peptide diffusion. The calculations have accounted for a hydration layer with an estimated depth of 2.8 Å.

Comparing the two, we see that adding the peptide to DPC corresponds to an increase in volume of ~25%, which is in agreement with similar studies of peptides in DPC micelles (*34*). The results show that the peptide forms a well-defined complex with the DPC molecules.

The intrinsic Trp fluorescence of Trp12 in HsapBK(233−260) was measured in DPC. A clear blue shift in the emission maximum as compared to what is expected for a solvent-exposed Trp residue was observed (341 nm for HsapBK(233−260) compared to 355 nm for a Trp residue in water) (*51*). This supports the diffusion results, and together with the fact that the peptide and micelle-bound DPC diffuse with the same diffusion constant, we conclude that the peptide is embedded in DPC. Very similar results have previously been observed for well-structured and tightly micelle-, bicelle-, or vesicle-bound peptides (*34*, *52*, *53*).

Solution Structure of HsapBK(233−260) in DPC. Two-dimensional COSY, NOESY, and TOCSY experiments were used to obtain resonance assignments for the peptide in DPC solution. In short, the assignment strategy was based on identifying spin systems in the TOCSY spectrum and connecting them together by sequential NOE patterns in the NOESY spectrum. The COSY spectrum was of little use, since the relatively broad peaks lead to cancellation of peaks. Approximately 90% of all ^{1}H atoms were assigned, including the side chain protons. Assignments for backbone H^N and H^α protons were found for all amino acid residues, except the N-terminal one. Most of the missing assignments were in side chains for which, e.g., H^β and H^γ protons overlapped. Secondary H^α chemical shifts were calculated according to the method of Wishart and Sykes (*54*) (Figure 2a).

For most of the peptide, secondary chemical shifts indicating helical structure are seen, with notable exceptions for residues Leu8, Asn9, and Gly14 and the termini. A solution structure for

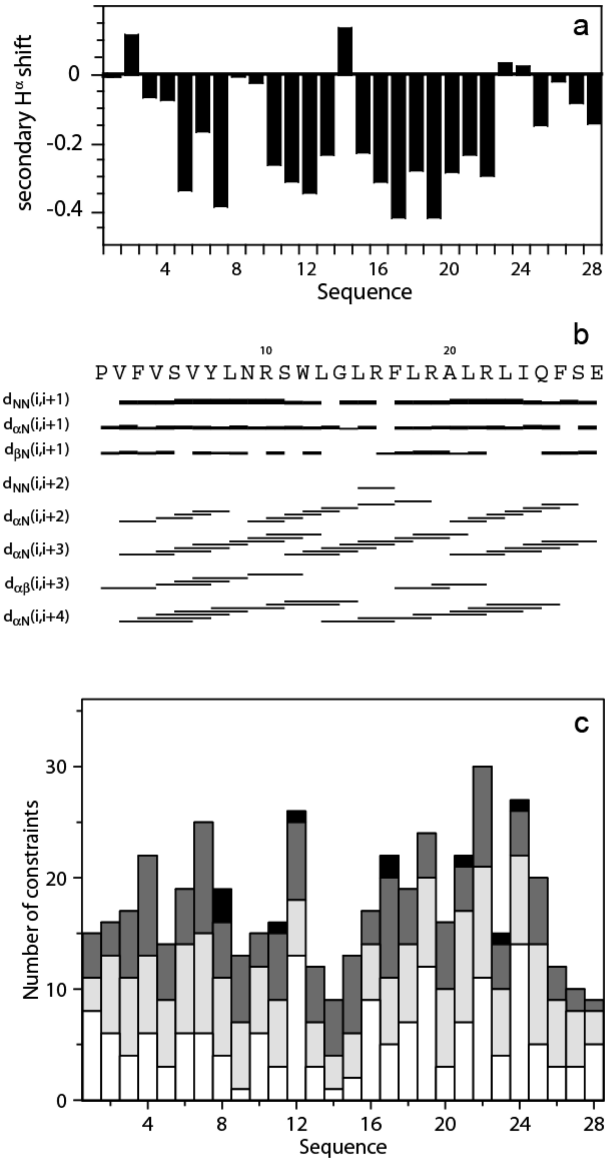

FIGURE 2: Structural data for HsapBK(233−260) in 100 mM DPC. (a) H^{α} secondary chemical shifts. (b) Summary of sequential and medium-range NOEs obtained from the NOESY spectrum recorded with a τ_{mix} of 150 ms. (c) Summary of the number of restraints for each amino acid residue: white for intraresidue, light gray for sequential, dark gray for medium-range, and black for long-range NOEs.

the peptide was calculated on the basis of 327 distance constraints derived from the two-dimensional NOESY with a mixing time of 150 ms. In agreement with the helical secondary shifts, many of the medium-range NOEs indicating helical structure were found throughout the peptide, although several were missing in the region between Leu8 and Asn9, Trp12 and Arg19, and Leu23 and Glu28 (Figure 2b).

A summary of the number of constraints per residue is given in Figure 2c. A few (six) unambiguous long-range NOEs were found, which are essential for folding the structure into a helix−turn−helix motif. Part of a NOESY spectrum displaying some of these cross-peaks is shown in Figure S1 (Supporting Information). These NOEs are seen between Leu8, Ser11, and Trp12 and Phe17, Leu21, Leu23, and Ile24 (Figure 3a,b). From the final round of calculations, an ensemble of 25 structures was selected to represent the solution structure (Figure 4). These structures have low CYANA target function and modest distance violations (Table 2).

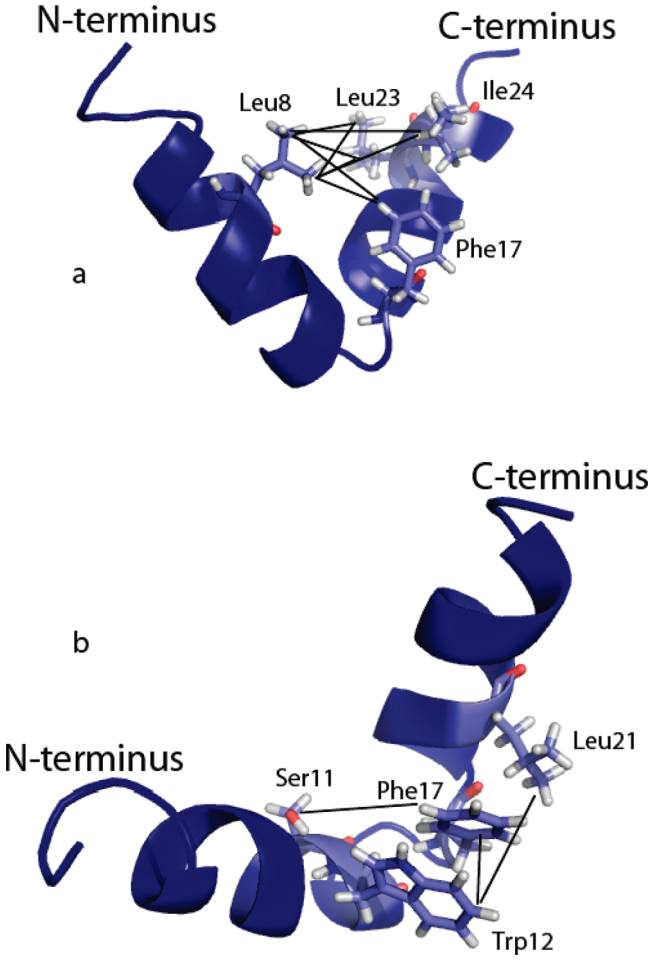

FIGURE 3: (a) Long-range NOEs were obtained between the methyl groups of Leu8 and the aromatic ring of Phe17 and the methyl groups of Leu23 and Ile24, respectively. (b) Long-range NOEs was also found between Trp12 and Phe17, between Trp12 and Leu21, and between Ser11 and Phe17.

The presented structure was calculated on the basis of only six unambiguous long-range constraints. Furthermore, these were all set conservatively to an upper distance limit of 6 Å in the calculation. The interface of the two helices is not as well-defined as the secondary structure, but since the number of long-range constraints is so few compared to the number of sequential and medium-range constraints, this will not be reflected in the rmsd values for atomic coordinates. To visualize this, a picture in which the upper distance limit for the long-range NOEs is varied is included (Figure 5). As one can see, the overall structure is retained as the number of constraints is increased or decreased, but the relative position of the two helices is varied. Furthermore, each of the long-range NOEs has been carefully examined, so that none one of them forces a specific tertiary structure by itself, which can be a problem in the case of a sparse NOE network. We calculated the structure by using one distance constraint at a time, which showed that the fold was not created by enforcing one single distance (Figure S2 of the Supporting Information).

To further validate the structure, we carefully examined the calculated structure to ensure that no significant long-range constraints were missing in the data. In particular, we looked for potential long-range distances of <6 Å. On the basis of measured distances in the structure, the side chain of Val4 is close to both Leu23 and Ile24; however, the chemical shift of the two methyl groups in Val4 overlaps with that of one of the methyl

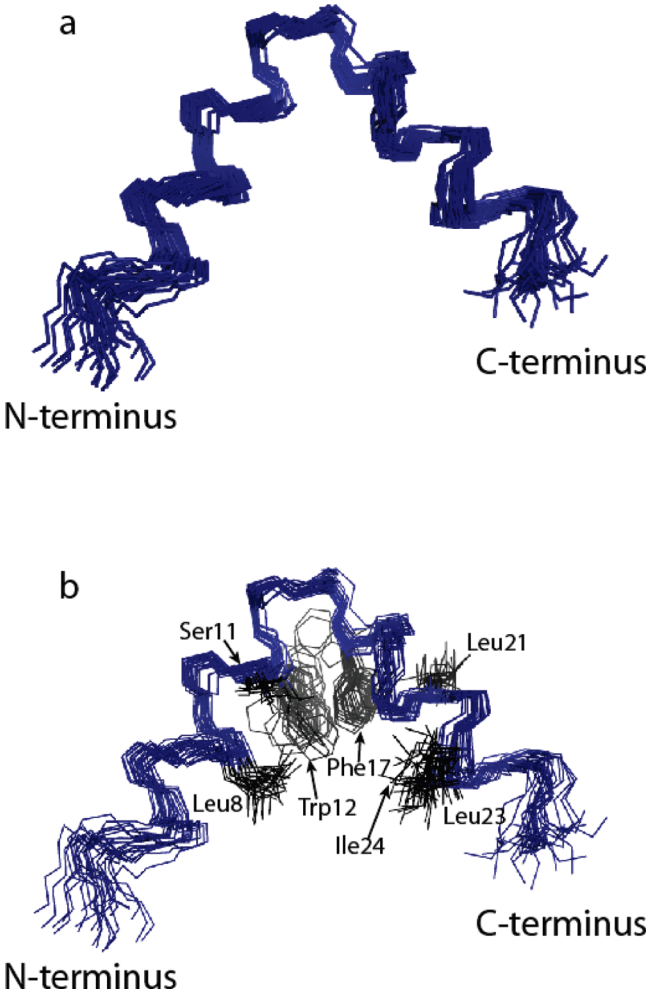

FIGURE 4: Solution structure of HsapBK(233−260) in 100 mM DPC as represented by an ensemble of the 25 structures with the lowest CYANA target function without (a) and with (b) the residues involved in long-range constraints. The structures were superimposed using backbone atoms in residues 5−14 and 18−26.

Table 2: Structural Statistics for the Ensemble of 25 Structures of HsapBK (233−260) in DPC Micelles

no. of constraints	327
Cyana target function	0.07 ± 0.03 Å^2
maximum distance violation	0.09 ± 0.04 Å
backbone atom rmsd (Å)	
all residues	0.83
residues 5−14	0.27
residues 18−26	0.14
residues 5−14, 18−26	0.60
Ramachandran plot regions (%)	
most favored	80.5
allowed region	18.2
generously allowed	1.3
disallowed	0

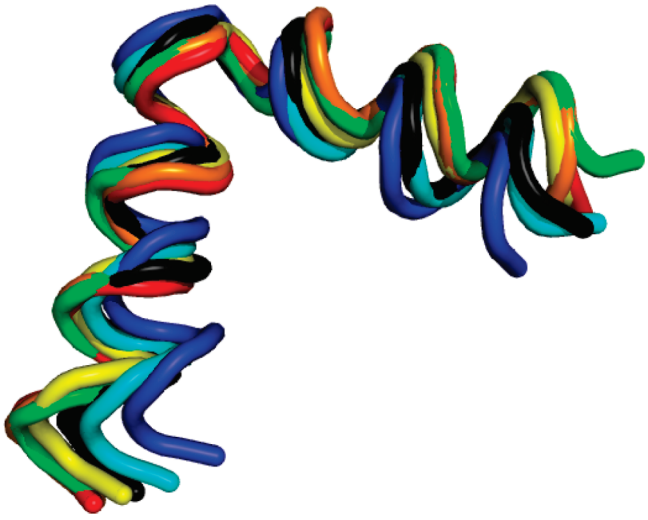

FIGURE 5: The interface between the two helices is not as well-defined as the secondary structure. To emphasize that, structures calculated with the long-range NOEs set to 5 Å (black), 5.5 Å (blue), 6 Å (cyan), 6.5 Å (green), 7 Å (yellow), 7.5 Å (orange), and 8 Å (red) are shown.

groups in Leu8 and in Leu18, and hence, we did not use these cross-peaks. The second unambiguously assigned methyl group resonance of Leu8 did, however, exhibit cross-peaks to Leu23, and this constraint was included.

Among other short distances between side chains in the structure, we note that Ser11 H^{β} protons are close to both Arg19 and Ala20 H^{β} protons. Cross-peaks corresponding to the chemical shifts of these protons can indeed be observed in the spectra, but the shifts of Arg19 and Ala20 overlap with other resonances in the peptide. Hence, no assignments were included.

Finally, several medium- and long-range distances between protons close to the turn of the structure should generate cross-peaks in the NOESY spectrum. Also here, the overlap is too severe to make unambiguous assignments. The overlap is mainly between methyl groups in Leu13 and Leu15 and between side chain protons in the Arg residues (Arg16 and Arg19). Gly14 had only very few inter-residue NOE cross-peaks (Figure 2c).

On the basis of analyses of backbone dihedral angles and the potential for forming helical hydrogen bonds, helical structure was assigned between residues Ser5 and Gly14 (N-terminal helix) and between Leu18 and Phe26 (C-terminal helix). Notably, the dihedral angles for Asn9 and Arg10 are not strictly α-helical. This is further supported by the lack of helical secondary shifts for these residues (Figure 2a) and may indicate a break in the N-terminal α-helix at this point. One should also note that residues 15−20 have dihedral angles within the α-helical region, but not in all structures within the ensemble. Analysis of the hydrogen bonding pattern was slightly more complicated. Regular α-helical hydrogen bonds, although weak, were found for most of the N-terminal helix, while hydrogen bonds were observed only for Ala20 with both Leu23 and Ile24, indicating the possibility of both NH(i)−O(i + 4) and NH(i)−O(i + 3) hydrogen bonding patterns. Hence, we conclude that the short C-terminal helix corresponding to S4 has irregular secondary structure, probably due to dynamic exchange between α-helical and 3_{10}-helical structure, but that the calculated backbone dihedral angles are within the α-helical region of the Ramachandran map for residues Leu18−Gln25.

The precision of the structure, as judged from rmsds in atomic coordinates, is fairly high, especially for the two helices (Table 2). The short turn between the two helices is defined by fewer distances, since NOE cross-peaks in this area are difficult to assign due to the extensive overlap in the spectrum (Figure 2c).

DISCUSSION

In this report, we have determined the solution structure of the putative S3b−S4 voltage-sensor paddle in the

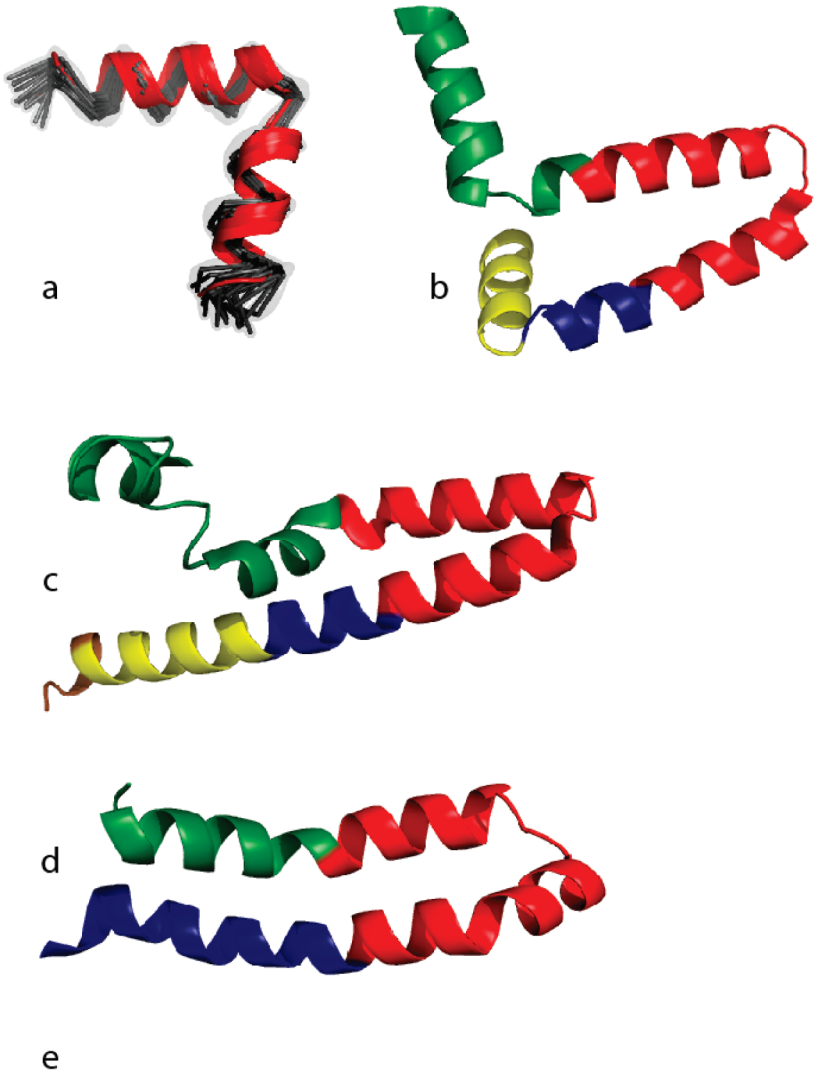

FIGURE 6: Comparison of the S3b−S4 sequence in HsapBK with the corresponding sequences from K_vAP and K_v1.2 channels. An overlay of all 25 structures for HsapBK(233−260) in the NMR-derived ensemble with the average structure colored red is shown in panel a. Panel b shows the S3−S4 fragment in the K_vAP structure (PDB entry 1ORQ). Panel c is from the structure of the isolated sensor in K_vAP (PDB entry 1ORS). Panel d shows the structure of the S3−S4 sequence in the rat K_v2.1 paddle chimera channel (PDB entry 2R9R). The region corresponding to the HsapBK S3b−S4 fragment is colored red in all structures. Connecting regions in the other structures are shown in different colors to facilitate comparison. A multiple-sequence alignment of the four sequences is shown in panel e, with the same color coding that is used in panels a−d. Completely conserved residues are marked with asterisks. Notably, the turn in the K_v2.1 channel is located in a different position than in the other structures.

voltage- and calcium-dependent HsapBK potassium channel. The isolated paddle in DPC micelles is here shown to form a structure in which two short helices interact to form a helix−turn−helix motif. On the basis of previous sequence alignments between the S3b−S4 motif in HsapBK and the K_vAP potassium channels, it is anticipated that the S3b helix spans residues 1−10 and that the S4 helix spans residues 12−27 (*5*) in HsapBK. In this study, we see that the N-terminal helix (corresponding to S3) of HsapBK(233−260) comprises residues Ser5−Gly14 and that the C-terminal helix (corresponding to S4) comprises residues Leu18−Phe26, although there is evidence, from both secondary chemical shifts and NOEs, that the C-terminal helix may comprise also residues preceding these (Leu15−Phe17).

Comparison of the structure of the HsapBK segment to those of crystal structures of K_v channels (*5*, *7*, *8*) shows that they are in part similar (Figure 6). The hydrophobic interactions between the two helices in this structure mainly involve Leu8, Ser11, Trp12, Phe17, Leu21, Leu23, and Ile24. Compared with other BK channels in different species, all residues in S3 and S4 in the proteins are completely conserved (*55*). Compared with the Shaker and K_v or Na_v channels, these residues are conservatively replaced with other aromatic and hydrophobic residues (*5*, *6*, *55*). However, Trp12 that participates in the

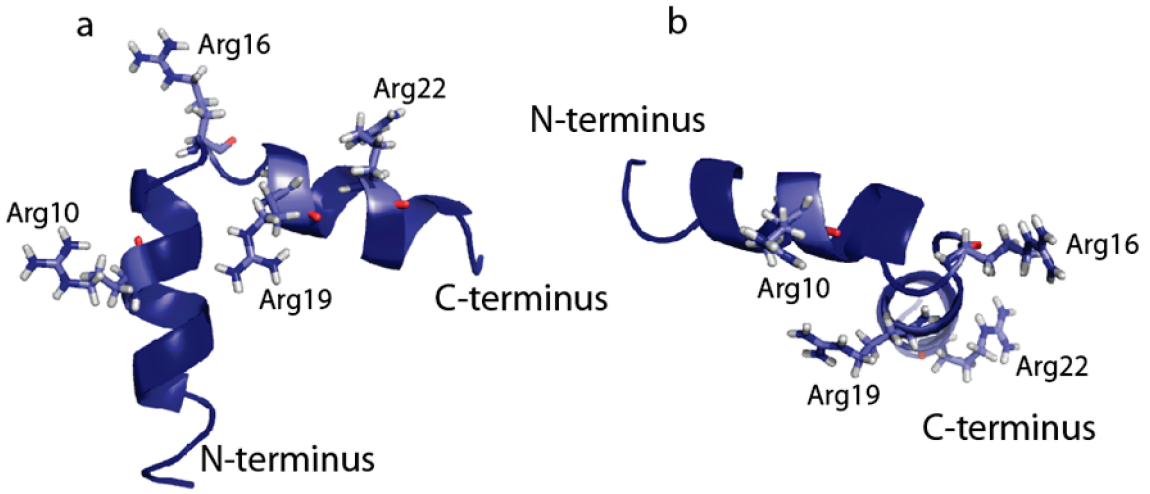

FIGURE 7: Solution structure of HsapBK(233−260). The side chains of the four Arg residues are shown. Panel a shows a front view, while panel b shows a view down along the C-terminal S4 helix, indicating that the Arg residues are all on the outside of the structure.

long-range contacts in this structure is not conserved in the K_vAP and K_v1.2 S3−S4 fragments (Figure 6). Furthermore, Gly14 in HsapBK(233−260) is located in the loop between the two helices and hence corresponds to the glycine-rich loop in K_vAP(112−146) and not to the S4 segment as suggested from ClustalW alignment (*5*). This is not a surprise, since structure is more evolutionarily conserved than primary sequence. The two helices in the HsapBK(233−260) structure presented here are much shorter, and not as well-packed as in other K_v structures. The K_v channels are predicted to have several residues in a loop region between the two helices, while this is not the case for BK channels. The S3b−S4 region of the human BK channels is furthermore predicted to be shorter than in the K_v channels.

As there are no structures of a full-length BK channel, we cannot determine whether the differences observed here are due to the DPC environment or the lack of the remaining protein or if they indeed are true differences. It is, however, important to note that this short fragment does indeed form a helix−turn−helix structure in the presence of a membrane mimetic and that the location of the S3b−S4 domain may differ somewhat in BK channels as compared to K_v channels, while the structural feature of the paddle is conserved.

It has been demonstrated that the voltage sensors can function on their own, in proteins without ion-conducting pores (*17*−*19*, *56*), and that the paddle domains in K_v and Na_v channels are modular and can be swapped between different ion channels (*57*−*59*). This supports the idea that the structure presented here represents a nativelike conformation of the paddle domain in BK channels.

The structure is embedded within a layer of DPC molecules, as evidenced from diffusion measurements, which serve as a model for the membrane. Several solution structures of membrane proteins and peptides in DPC, as well as in other detergents, have been determined (*34*, *44*, *60*−*62*), indicating that the DPC provides a reasonable environment for investigating structure. Many proteins retain their nativelike structure and activity in such solvents. It should, however, be said that there are also protein fragments that do not adopt their native structure in micellar environments. These are often surface-associated protein motifs, or peptides (*44*, *62*), for which the structure depends critically on the membrane surface.

The four Arg residues within the peptide have been implicated in the gating properties of the voltage-sensor motif, which has been shown by various biophysical techniques (*23*−*25*, *63*). The extent to which these Arg residues move across the lipid bilayer has, however, been debated. MacKinnon's group has shown that the paddle is highly mobile (*63*). Furthermore, the crystal structure of a chimaeric channel in a lipid environment revealed that the charges are exposed to the lipid phosphates in the membrane, and that charge stabilization may occur through interactions with negatively charged residues (*8*). It has also been demonstrated that the isolated S4 helix from K_vAP, containing most of the Arg residues, can be inserted in a membrane in a transmembrane way and that the charges are stabilized by interactions with the lipid phosphates (*64*, *65*). Molecular dynamics simulations of the voltage-sensor domain have shown that at least some of the Arg residues in the voltage-sensor domain are not exposed to the hydrophobic interior of the bilayer (*66*−*68*). It has been suggested that the paddle undergoes considerable motion and that the gating involves changing the bilayer and water exposure of the S3b−S4 paddle (*66*). It has also been shown that the membrane may be affected by the sensor, leading to a decrease in the hydrophobic thickness of the bilayer (*66*, *69*). Here we see that three of the Arg residues are located in the putative S4 part of the fragment, and all are more or less exposed on the surface of the structure (Figure 7). The fourth Arg residue is situated close to the C-terminus of the N-terminal helix, and its side chain is also exposed. This may in part be due to the nature of the membrane mimetic but still shows that the fragment forms a structure with exposed Arg residues.

Another interesting observation is that the C-terminal helix in HsapBK(233−260), corresponding to S4, seems to be able to adopt (partially) a 3_{10}-helical conformation. This has been implicated in being part of the gating mechanism (*8*, *66*, *69*, *70*), in which the change in conformation is associated with the movement between the resting and activated states.

The solution structure of the sequence derived from the HsapBK channel in this investigation clearly shows that a helix−turn−helix conformation is formed and that further studies of the motion and membrane interactions of this motif in more nativelike membrane environments, such as phospholipid bicelles, are feasible. Future studies of mobility and, in particular, the response to membrane potential will together with

the structure presented here reveal important insights into the dynamics of this sequence and of movements within a bilayer and reveal details in membrane interactions of the voltage-sensor paddle.

ACKNOWLEDGMENT

We thank the Swedish NMR Centre for access to the NMR spectrometers.

SUPPORTING INFORMATION AVAILABLE

Figures showing parts of a two-dimensional NOESY spectrum and the result of individual long distance constraints on the structure. This material is available free of charge via the Internet at http://pubs.acs.org.

REFERENCES

(1) Hodgin, A. L., and Huxley, A. F. (1952) A Quantitative Description of Membrane Current and its Application to Conduction and Excitation in Nerve. *J. Physiol. 117, 500–544*.
(2) Jan, L. Y., and Jan, Y. N. (1997) Voltage-Gated and Inwardly Rectifying Potassium Channels. *J. Physiol. 505 (Part 2), 267–282*.
(3) Miller, C. (2000) An Overview of the Potassium Channel Family. *Genome Biol. 1, 0004.1–0004.5*.
(4) Bezanilla, F. (2000) The Voltage Sensor in Voltage-Dependent Ion Channels. *Physiol. Rev. 80, 555–592*.
(5) Jiang, Y., Lee, A., Chen, J., Ruta, V., Cadene, M., Chait, B. T., and MacKinnon, R. (2003) X-ray Structure of a Voltage-Dependent K Channel. *Nature 423, 33–41*.
(6) Long, S. B., Campbell, E. B., and Mackinnon, R. (2005) Crystal Structure of a Mammalian Voltage-Dependent Shaker Family K^+ Channel. *Science 309, 897–903*.
(7) Lee, S. Y., Lee, A., Chen, J., and MacKinnon, R. (2005) Structure of the KvAP Voltage-Dependent K^+ Channel and its Dependence on the Lipid Membrane. *Proc. Natl. Acad. Sci. U.S.A. 102, 15441–15446*.
(8) Long, S. B., Tao, X., Campbell, E. B., and MacKinnon, R. (2007) Atomic Structure of a Voltage-Dependent K^+ Channel in a Lipid Membrane-Like Environment. *Nature 450, 376–382*.
(9) Meera, P., Wallner, M., Song, M., and Toro, L. (1997) Large Conductance Voltage- and Calcium-Dependent K^+ Channel, a Distinct Member of Voltage-Dependent Ion Channels with Seven N-Terminal Transmembrane Segments (S0-S6), an Extracellular N Terminus, and an Intracellular (S9-S10) C Terminus. *Proc. Natl. Acad. Sci. U.S.A. 94, 14066–14071*.
(10) Marty, A. (1981) Ca-Dependent K Channels with Large Unitary Conductance in Chromaffin Cell Membranes. *Nature 291, 497–500*.
(11) Pallotta, B. S., Magleby, K. L., and Barrett, J. N. (1981) Single Channel Recordings of Ca^{2+}-Activated K^+ Currents in Rat Muscle Cell Culture. *Nature 293, 471–474*.
(12) Latorre, R., Vergara, C., and Hidalgo, C. (1982) Reconstitution in Planar Lipid Bilayers of a Ca^{2+}-Dependent K^+ Channel from Transverse Tubule Membranes Isolated from Rabbit Skeletal Muscle. *Proc. Natl. Acad. Sci. U.S.A. 79, 805–809*.
(13) Ghatta, S., Nimmagadda, D., Xu, X., and O'Rourke, S. T. (2006) Large-Conductance, Calcium-Activated Potassium Channels: Structural and Functional Implications. *Pharmacol. Ther. 110, 103–116*.
(14) Bezanilla, F. (2002) Voltage Sensor Movements. *J. Gen. Physiol. 120, 465–473*.
(15) Noda, M., Ikeda, T., Suzuki, H., Takeshima, H., Takahashi, T., Kuno, M., and Numa, S. (1986) Expression of Functional Sodium Channels from Cloned cDNA. *Nature 322, 826–828*.
(16) Murata, Y., Iwasaki, H., Sasaki, M., Inaba, K., and Okamura, Y. (2005) Phosphoinositide phosphatase activity coupled to an intrinsic voltage sensor. *Nature 435, 1239–1243*.
(17) Ramsey, I. S., Moran, M. M., Chong, J. A., and Clapham, D. E. (2006) A Voltage-Gated Proton-Selective Channel Lacking the Pore Domain. *Nature 440, 1213–1216*.
(18) Sasaki, M., Takagi, M., and Okamura, Y. (2006) A Voltage Sensor-Domain Protein is a Voltage-Gated Proton Channel. *Science 312, 589–592*.
(19) Tombola, F., Ulbroch, M. H., and Isacoff, E. Y. (2008) The voltage-gated proton channel Hv1 has two pores, each controlled by one voltage sensor. *Neuron 58, 546–556*.
(20) Doyle, D. A., Cabral, J. M., Pfuetzner, R. A., Kuo, A., Gulbis, J. M., Cohen, S. L., Chait, B. T., and MacKinnon, R. (1998) The Structure of the Potassium Channel: Molecular Basis of K Conduction and Selectivity. *Science 280, 69*.
(21) Jiang, Y., Lee, A., Chen, J., Cadene, M., Chait, B. T., and MacKinnon, R. (2002) The Open Pore Conformation of Potassium Channels. *Nature 417, 523–526*.
(22) Kuo, A., Gulbis, J. M., Antcliff, J. F., Rahman, T., Lowe, E. D., Zimmer, J., Cuthbertson, J., Ashcroft, F. M., Ezaki, T., and Doyle, D. A. (2003) Crystal Structure of the Potassium Channel KirBac1.1 in the Closed State. *Science 300, 1922–1926*.
(23) Jiang, Y., Ruta, V., Chen, J., Lee, A., and MacKinnon, R. (2003) The Principle of Gating Charge Movement in a Voltage-Dependent K Channel. *Nature 423, 42–48*.
(24) Cuello, L. G., Cortes, D. M., and Perozo, E. (2004) Molecular Architecture of the KvAP Voltage-Dependent K^+ Channel in a Lipid Bilayer. *Science 306, 491–495*.
(25) Posson, D. J., Ge, P., Miller, C., Bezanilla, F., and Selvin, P. R. (2005) Small vertical movement of a K channel voltage sensor measured with luminescence energy transfer. *Nature 436, 848–851*.
(26) Jeener, J. (1971) Thesis, Ampere Summer School, Basko Polje, Yugoslavia.
(27) Aue, W., Bartholdi, E., and Ernst, R. (1976) Two-Dimensional Spectroscopy. Application to Nuclear Magnetic Resonance. *J. Chem. Phys. 64, 2229*.
(28) Braunschweiler, L., and Ernst, R. R. (1983) Coherence Transfer by Isotropic Mixing: Application to Proton Correlation Spectroscopy. *J. Magn. Reson. 53, 8*.
(29) Jeener, J., Meier, B. H., Bachmann, P., and Ernst, R. R. (1979) Investigation of Exchange Processes by Two-Dimensional NMR Spectroscopy. *J. Chem. Phys. 71, 4546–4553*.
(30) Papadopoulos, E., Oglecka, K., Mäler, L., Jarvet, J., Wright, P. E., Dyson, H. J., and Gräslund, A. (2006) NMR solution structure of the peptide fragment 1−31, derived from unprocessed mouse doppel protein, in DHPC micelles. *Biochemistry 45, 159–166*.
(31) Piotto, M., Saudek, V., and Sklenár, V. (1992) Gradient-Tailored Excitation for Single-Quantum NMR Spectroscopy of Aqueous Solutions. *J. Biomol. NMR 2, 661–665*.
(32) Delaglio, F., Grzesiek, S., Vuister, G. W., Zhu, G., Pfeifer, J., and Bax, A. (1995) NMRPipe: A Multidimensional Spectral Processing System Based on UNIX Pipes. *J. Biomol. NMR 6, 277–293*.
(33) Goddard, T. D., and Kneller, D. G. (1999) Sparky 3, University of California, San Francisco.
(34) Kallick, D. A., Tessmer, M. R., Watts, C. R., and Li, C. Y. (1995) The use of Dodecylphosphocholine Micelles in Solution NMR. *J. Magn. Reson., Ser. B 109, 60–65*.
(35) Stejskal, E. O., and Tanner, J. E. (1965) Spin Diffusion Measurements: Spin Echoes in the Presence of a Time Dependent Field Gradient. *J. Chem. Phys. 42, 288–292*.
(36) von Meerwall, E., and Kamat, M. (1989) Effect of Residual Field Gradients on Pulsed Gradient NMR Diffusion Measurements. *J. Magn. Reson. 83, 309–323*.
(37) Callaghan, P., Komlosh, M., and Nydén, M. (1998) High Magnetic Field Gradient PGSE NMR In the Presence of a Large Polarizing Field. *J. Magn. Reson. 133, 177–182*.
(38) Damberg, P., Jarvet, J., and Gräslund, A. (2001) Accurate Measurement of Translational Diffusion Coefficients: A Practical Method to Account for Nonlinear Gradients. *J. Magn. Reson. 148, 343–348*.
(39) Longsworth, L. G. (1960) The Mutual Diffusion of Light and Heavy Water. *J. Phys. Chem. 64, 1914–1917*.
(40) Andersson, A., Almqvist, J., Hagn, F., and Mäler, L. (2004) Diffusion and dynamics of penetratin in different membrane mimicking media. *Biochim. Biophys. Acta 1661, 18–25*.
(41) Price, W. S. (1997) Pulsed-field gradient nuclear magnetic resonance as a tool for studying translational diffusion: Part 1. Basic theory. *Concepts Magn. Reson. 9, 299–336*.
(42) Cantor, C. R., and Schimmel, P. R. (1980) Biophysical Chemistry, W. H. Freeman, San Fransisco.
(43) Guntert, P., Mumenthaler, C., and Wuthrich, K. (1997) Torsion Angle Dynamics for NMR Structure Calculation with the New Program DYANA. *J. Mol. Biol. 273, 283–298*.
(44) Andersson, A., and Mäler, L. (2002) NMR Solution Structure and Dynamics of Motilin in Isotropic Phospholipid Bicellar Solution. *J. Biomol. NMR 24, 103–112*.
(45) Laskowski, R. A., MacArthur, M. W., Moss, D. S., and Thornton, J. M. (1993) PROCHECK: A Program to Check the Stereochemical Quality of Protein Structures. *J. Appl. Crystallogr. 26, 283–291*.
(46) Sanders, C. R., and Sonnichsen, F. (2006) Solution NMR of Membrane Proteins: Practice and Challenges. *Magn. Reson. Chem. 44, S24–S40*.

(47) Lind, J., Nordin, J., and Maler, L. (2008) Lipid Dynamics in Fast-Tumbling Bicelles with Varying Bilayer Thickness: Effect of Model Transmembrane Peptides. *Biochim. Biophys. Acta 1778, 2526–2534*.
(48) Lindman, B., Puyal, M., Kamenka, N., Rymdén, R., and Stilbs, P. (1984) Micelle Formation of Anionic and Cationic Surfactants from Fourier Transform Hydrogen-1 and Lithium-7 Nuclear Magnetic Resonance and Tracer Self-Diffusion Studies. *J. Phys. Chem. 88, 5048–5057*.
(49) Lauterwein, J., Bosch, C., Brown, L. R., and Wuthrich, K. (1979) Physicochemical Studies of the Protein-Lipid Interactions in Melittin-Containing Micelles. *Biochim. Biophys. Acta 556, 244–264*.
(50) Gao, X., and Wong, T. C. (1998) Studies of the Binding and Structure of Adrenocorticotropin Peptides in Membrane Mimics by NMR Spectroscopy and Pulsed-Field Gradient Diffusion. *Biophys. J. 74, 1871–1888*.
(51) Lakowicz, J. R. (1999) Principles of Fluorescence Spectroscopy, Kluwer Academic Press, New York.
(52) Bárány-Wallje, E., Andersson, A., Gräslund, A., and Mäler, L. (2006) Dynamics of Transportan in Bicelles is Surface Charge Dependent. *J. Biomol. NMR 35, 137–147*.
(53) Magzoub, M., Kilk, K., Eriksson, L. E. G., Langel, U., and Gräslund, A. (2001) Interaction and structure induction of cell-penetrating peptides in the presence of phospholipid vesicles. *Biochim. Biophys. Acta 1512, 77–89*.
(54) Wishart, D. S., and Sykes, B. D. (1994) Chemical Shifts as a Tool for Structure Determination. *Methods Enzymol. 239, 363–392*.
(55) Ma, Z., Wong, K. Y., and Horrigan, F. T. (2008) An extracellular Cu^{2+} binding site in the voltage sensor of BK and Shaker potassium channels. *J. Gen. Physiol. 131, 483–502*.
(56) Freites, J. F., Tobias, D. J., and White, S. H. (2006) A voltage-sensor water pore. *Biophys. J. 91, L90–L92*.
(57) Alabi, A. A., Bahamonde, M. I., Jung, H. J., Kim, J. I., and Swartz, K. J. (2007) Portability of paddle motif function and pharmacology in voltage sensors. *Nature 450, 370–375*.
(58) Bosmans, F., Martin-Euclaire, M.-F., and Swartz, K. J. (2008) Deconstructing voltage sensor function and pharmacology in sodium channels. *Nature 456, 202–208*.
(59) Swartz, K. J. (2008) Sensing voltage across lipid membranes. *Nature 456, 891–897*.
(60) Arora, A., Abildgaard, F., Bushweller, J. H., and Tamm, L. K. (2001) Structure of Outer Membrane Protein A Transmembrane Domain by NMR Spectroscopy. *Nat. Struct. Biol. 8, 334–338*.
(61) Tamm, L. K., and Liang, B. (2006) NMR of Membrane Proteins in Solution. *Prog. Nucl. Magn. Reson. Spectrosc. 48, 201–210*.
(62) Chou, J. J., Kaufman, J. D., Stahl, S. J., Wingfield, P. T., and Bax, A. (2002) Micelle-Induced Curvature in a Water-Insoluble HIV-1 Env Peptide Revealed by NMR Dipolar Coupling Measurement in Stretched Polyacrylamide Gel. *J. Am. Chem. Soc. 124, 2450–2451*.
(63) Ruta, V., Chen, J., and MacKinnon, R. (2005) Calibrated Measurement of Gating-Charge Arginine Displacement in the KvAP Voltage-Dependent K^+ Channel. *Cell 123, 463–475*.
(64) Hessa, T., White, S. H., and von Heijne, G. (2005) Membrane insertion of a potassium-channel voltage sensor. *Science 307, 1427–1427*.
(65) Freites, J. A., Tobias, D. J., von Heijne, G., and White, S. H. (2005) Interface connections of a transmembrane voltage sensor. *Proc. Natl. Acad. Sci. U.S.A. 102, 15059–15064*.
(66) Sands, Z. A., Grottesi, A., and Sansom, M. S. P. (2006) The intrinsic flexibility of the Kv voltage sensors and its implications for channel gating. *Biophys. J. 90, 1598–1606*.
(67) Treptow, W., and Tarek, M. (2006) Environment of the gating charges in the Kv1.2 Shaker potassium channel. *Biophys. J. 90, L64–L66*.
(68) Jogini, V., and Roux, B. (2007) Dynamics of the Kv1.2 voltage-gated K^+ channel in a membrane environment. *Biophys. J. 93, 3070–3082*.
(69) Bjelkmar, P., Niemelä, P. S., Vattulainen, I., and Lindahl, E. (2009) Conformational changes and slow dynamics through microsecond polarized atomistic molecular simulation of an integral Kv1.2 ion channel. *PLoS Comput. Biol. 5, No. e1000289*.
(70) Villalba-Galea, C. A., Sandtner, W., Starace, D. M., and Bezanilla, F. (2008) S4-based voltage sensors have three major conformations. *Proc. Natl. Acad. Sci. U.S.A. 105, 17600–17607*.